Misregistration impacts on hyperspectral target detection

Jason T. Casey[a] and John P. Kerekes[b]
[a]Logos Technologies, 3811 N. Fairfax Drive, Suite 100, Arlington, Virginia 22203, USA
JasonTCasey@gmail.com
[b]Chester F. Carlson Center for Imaging Science, Rochester Institute of Technology, 54 Lomb Memorial Drive, Rochester, New York 14623, USA,
kerekes@cis.rit.edu

Abstract. Hyperspectral imaging sensors commonly employ multiple apertures or focal planes for broad spectral coverage. These designs often result in spatial misregistration artifacts between the spectral regions. Unknown misregistration errors of fractions of a pixel cannot be corrected and can have a negative impact on target detection performance, especially for targets that are subpixel. The work here analyzes the impact of band-to-band misregistration on hyperspectral target detection performance. Synthetic imagery was used to simulate various amounts of sub-pixel misregistration between the visible (VIS) and near infrared (NIR) regions of the optical spectrum. Scenes were created with vehicles placed as targets. Target detection algorithms were applied using both the full spectrum misregistered imagery, and the VIS and NIR bands separately. Receiver operating characteristic curves were used to assess the performance of each algorithm for each target. Results indicate that statistical target detection algorithms are less sensitive to band-to-band misregistration than geometric algorithms. Results also indicate that in some cases it is more beneficial to use full spectrum misregistered imagery rather than applying target detection algorithms to the VIS and NIR bands separately, even for large amounts of sub-pixel misregistration.

Keywords: hyperspectral imaging, target detection, misregistration.

1 INTRODUCTION

It is common for hyperspectral imaging sensors to rely on the use of multiple apertures or focal planes to span a broad spectral range due to limitations in detector technology [1-3]. This technique allows for imaging with more spectral bands than would be possible using a single focal plane technology. The problem with this approach, however, is imperfect image registration. The resulting composite hypercube consists of independent hyperspectral images collected at each focal plane which are generally not perfectly registered to one another. Also, even instruments using a single aperture and focal plane can suffer from inherent misregistrations due to the optical characteristics of the spectrometers [4].

Misregistration between sets of spectral bands has a negative impact on target detection performance, particularly when detecting small or subpixel targets because there is a different amount of spectral mixing of target and background materials in each set of spectral bands. This paper focuses on target detection performance using simulated band-to-band misregistered imagery. Synthetic imagery was used to allow full knowledge and precise control of the amount of misregistration. Synthetic images were created at various amounts of misregistration between the visible and near infrared bands. An urban scene was populated with 140 vehicles placed in different types of background materials. Three different target detection algorithms were applied to the misregistered imagery, as well as to the visible (VIS) and near infrared (NIR) hyperspectral images separately. Receiver Operator Characteristic (ROC) curves were generated to compare the target detection performance of various

Received 1 Aug 2008; accepted 17 Feb 2009; published 24 Feb 2009 [CCC: 19313195/2009/$25.00]

algorithms. ROC curves show the tradeoff in probability of detection versus probability of false alarm as a detection threshold is varied [5].

The motivation for this research is in part due to a characteristic of a hyperspectral sensor used at the Rochester Institute of Technology (RIT). RIT's Modular Imaging Spectrometer Instrument (MISI) is a hyperspectral line scanner that employs two spectrometers, one with 35 spectral channels in the VIS and one with 35 spectral channels in the NIR, each fed by its own optical fiber from the focal plane [2]. This two-fiber configuration causes a misregistration between the VIS and NIR bands since the fibers occupy different locations on the focal plane. Also, MISI's line scanning optical design causes the amount of misregistration to vary as it scans over the scene. More information on MISI's misregistration issue and correction techniques can be found in [6]. Another example of an imaging system suffering misregistration between sets of spectral bands is NASA's EO-1 Hyperion [3]. Hyperion has a misregistration of approximately 0.28 pixels between the visible near infrared (VNIR) and the shortwave infrared (SWIR) bands due to the fact they are imaged by separate focal planes that are not perfectly co-aligned. The following sections report on the image simulation, the algorithms used in the evaluation, the results and our conclusions.

Fig. 1. RIT's Modular Imaging Spectrometer Instrument, a hyperspectral line scanner.

a) b)

Fig. 2. Illustration of MISI's focal plane (a). VIS and NIR channels are off the center axis. This results in a slight misregistration between the VIS and NIR channels shown in (b).

2 SYNTHETIC IMAGE GENERATION

This section describes the image simulation tool used to generate the synthetic imagery, the particular scene used for the study, and the methodology used to create the misregistered images.

2.1 Image simulation tool

The image simulation was performed using the Digital Imaging and Remote Sensing Image Generation (DIRSIG) tool. DIRSIG [7] is a first principles based synthetic image generation model developed by the Digital Imaging and Remote Sensing Laboratory (DIRS) at RIT. It is capable of producing radiometrically accurate broad band panchromatic, multispectral, and hyperspectral images from the visible through thermal infrared regions of the optical spectrum. DIRSIG uses radiation propagation and geometric submodels to model such effects as the scene-sun-sensor geometry, the sensor point spread function (PSF), and the bidirectional reflectance distribution function (BRDF) of materials. The Air Force Research Laboratory's Moderate resolution atmospheric transmission code (MODTRAN [8]) is used to model the propagation of electromagnetic radiation through the atmosphere.

2.2 Scene

A portion of an existing large urban area scene known as MegaScene [9] was selected for this study. This scene was modeled after an urban residential area just northeast of Rochester, New York. The area includes residential neighborhoods, parks, and a school complex as shown in Figure 3. The ground size of the scene is approximately 800 meters by 800 meters. A running track is located near the bottom of the scene and two large calibration panels (light and dark) were placed in the infield of the model scene. DIRSIG was used to generate this radiometrically accurate scene. Physical models were used to simulate a 3-d environment complete with various surfaces, buildings, trees, and vehicles. Spectral reflectance curves from the DIRSIG reference library were applied to each surface in the scene. MODTRAN was used to model all propagation of electromagnetic radiation through the atmosphere until it is collected by the sensor. All of this was done to simulate a real HSI collection. After the simulated scene was imaged, a common HSI processing approach was followed and the image was atmospherically compensated to spectral reflectance using the two large calibration panels inside the track area and the empirical line method (ELM) [10]. Three versions of the scene were generated, each with vehicles having different spectral reflectance curves corresponding to their color (blue, green, or white). 140 vehicles (of the same color) were placed in each scene to provide sufficient samples to estimate detection probability. To allow for a range of backgrounds, the vehicles were placed either on grass, the running track or on one of two types of road asphalt. Target masks were created which labeled pixels as target or background. These masks were used to calculate the probability of detection and probability of false alarm to generate ROC curves after target detection algorithms were applied to the images. Further details are available in [6].

2.3 Model sensor and misregistered image simulation

A notional model of an airborne hyperspectral imager was implemented within DIRSIG to render the at-sensor radiance generated by the scene and atmospheric models as a hyperspectral image. The model sensor had 73 bands with 10 nm spectral resolution and spaced every 10 nm from 0.40 to 1.12 microns. The first 31 (0.40 to 0.70 microns) were considered to be from one spectrometer (VIS) while the remaining 42 (0.71 to 1.12 microns) were considered to be from a second spectrometer (NIR) and shifted spatially to create the misregistration as described below. All final images had Gaussian random noise added to achieve an average signal-to-noise ratio (SNR) of 100 for all spectral bands.

The scene was initially rendered at a ground sample spacing of 0.2 meters, yielding images that were 4000 x 4000 for the scene. These images were then spatially degraded using a circularly symmetric Gaussian point spread function (PSF) to yield pixels spaced 2 meters apart with approximately 2 meter resolution. To induce misregistration, the NIR bands were shifted by integer increments of the initial 0.2 meter pixels relative to the VIS bands prior to

the application of the Gaussian. The 10x oversampling in the initial rendering allowed misregistrations to be created in 0.1 pixel increments for the final 400 x 400 pixel images. Misregistrations between the VIS and NIR image cubes of up to 0.5 pixels in one direction were studied. Figure 4 shows a natural color rendition of a small portion of the initial image and the same area of the final image after the point spread function was applied. As can be seen the vehicles occupy a portion of several pixels in the 2 meter images used for the detection studies. Figure 5 shows reflectance curves for the vehicles used in this simulation.

Fig. 3. Natural color (RGB) rendition of the scene used in this study. Red dots indicate the locations of the vehicles used as targets.

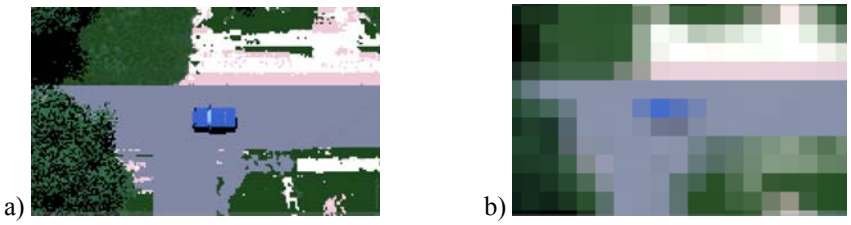

Fig. 4. Natural color (RGB) images of a small area of the scene rendered at the a) initial high resolution and b) after application of the Gaussian PSF.

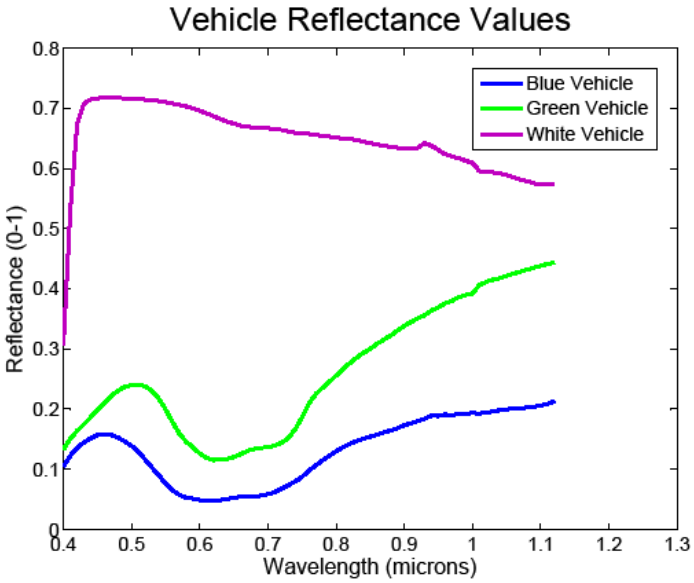

Fig. 5. Reflectance values of the three vehicles used in the simulation.

3 TARGET DETECTION ALGORITHMS AND PERFORMANCE EVALUATION

Three target detection algorithms were considered in this study: the Spectral Angle Map (SAM) [11], the Adaptive Subspace Detector (ASD) [12] and the Adaptive Coherence Estimator (ACE) [13]. These algorithms have been put in a common notation for the hyperspectral imaging community in [14]. They were selected as commonly used representative algorithms to study the influence of the algorithm on detection errors introduced by the misregistration. SAM and ASD are examples of geometric algorithms, with the difference being ASD uses information about the background while SAM does not. ACE is a stochastic detection algorithm which uses the image-wide background covariance. These three algorithms are commonly used in the hyperspectral target detection community and were selected to form a good representation of the geometrical and statistical classes of algorithms. All were applied in the reflectance domain to atmospherically compensated versions of the imagery generated using ELM and the large calibration panels inside the running track.

The SAM algorithm given in Eq. (1) uses no background information and relies solely on the target signature to detect targets. Here, d is the target library spectral reflectance pixel vector and x is a test pixel vector from the reflectance image. The superscript T denotes transpose.

$$T_{SAM}(x) = \frac{d^T x}{\left(d^T d\right)^{1/2}\left(x^T x\right)^{1/2}} \tag{1}$$

The ASD algorithm, given in Eq. (2), uses scene endmembers to characterize the background.

$$T_{ASD}(x) = \frac{x^T (P_b - P_s) x}{x^T P_s x} \tag{2}$$

Here, P_b is a matrix specifying the background space and P_s is the corresponding matrix for the image space. The background and image matrices are computed using Eq. (3)

$$P_y = \left(I - M_y M_y^{\#}\right) \tag{3}$$

where I is the identity matrix, M is a matrix of endmembers, and y specifies which endmembers are used to construct M. $M^{\#}$ is the pseudo inverse of M and is shown in Eq. (4).

$$M^{\#} = \left(M^T M\right)^{-1} M^T \tag{4}$$

P_b uses a matrix of only background endmembers when constructing M_b and P_s uses a matrix of background endmembers concatenated with a matrix of target endmembers for M_s. The background endmembers were obtained as the cluster centers (in spectral space) found from an unsupervised K-means clustering algorithm applied to the image assuming six classes. Multiple target endmembers may be used depending on how the target signature is expected to vary under different conditions. However, in this study only one target endmember was used as the retrieved target signatures were not expected to vary much throughout the scene.

The ACE algorithm is a stochastic algorithm and uses a covariance matrix to characterize the background. In this experiment, the target-free, mean subtracted, image-wide covariance was used. ACE is a variation of the generalized likelihood ratio test (GLRT) and is given in Eq. (5)

$$T_{ACE}(x) = \frac{(d^T \Sigma_b^{-1} x)^2}{(d^T \Sigma_b^{-1} d)(x^T \Sigma_b^{-1} x)} \tag{5}$$

where Σ_b is the target-free, image-wide, mean subtracted covariance matrix and d and x are defined as above.

For each algorithm and test image, scalar test statistic images $T(x)$ were generated for all pixels x using the equations provided above. ROC curves were generated by varying a detection threshold from $-\infty$ to $+\infty$ and recording the observed probability of detection and probability of false alarm at each threshold. The probability of detection is estimated as the ratio of the number of true target vehicles detected divided by the total number of true target vehicles. A vehicle was counted as being detected if the maximum test statistic value within the pixels occupied by the target vehicle exceeds the threshold. The probability of false alarm was estimated as the ratio of the number of non-target pixels (background) whose test statistic exceeded the threshold divided by the total number of non-target pixels in the image. Varying the threshold shows the tradeoff in probability of detection versus false alarm. ROC curves were generated for each level of band-to-band misregistration to illustrate how misregistration affects target detection performance. As described above, in generating the ROC curves estimates of the probability of detection were made on a per-target basis while estimates of the false alarm probability were per-pixel excluding a small buffer region around each target.

4 RESULTS

ROC curves were created from the target detection maps resulting from applying the SAM, ASD and ACE target detection algorithms on each scene. In addition to applying the algorithms to the full spectrum including various amounts of misregistration, the algorithms were also applied to only the VIS or NIR spectral subsets. ROC curve results from the SAM algorithm applied to the scenes with blue vehicles and the various misregistration levels are shown in Figure 6. Figures 7 and 8 show corresponding curves obtained using the ASD and ACE algorithms, respectively. Similar results were observed for the green and white vehicles and are available in [6]. Figure 9 shows the probability of detection at a constant false alarm rate (CFAR) of 10^{-4} for the blue vehicle and the various combinations of misregistration and algorithms. Figures 10 and 11 show the corresponding results for the green and white vehicles.

A visual inspection of the ROC curves and detection rate graphs reveals that SAM and ASD tend to be more sensitive to band-to-band misregistration than ACE. ASD also does not appear to gain benefits of using the entire, slightly misregistered spectrum. ACE tends to be the most robust in the presence of misregistration and using all bands in the spectral range yields performance increases over using only the VIS or NIR regions of the spectrum, even at misregistration amounts up to 0.3 pixels or more.

For the three vehicles used in this experiment, SAM and ASD tended to have higher detection rates when using either the VIS or NIR bands separately, rather than using the full spectrum, even at small amounts of misregistration. While ACE sometimes has lower overall detection rates, it tended to have higher detection rates relative to using only the VIS or NIR bands separately even at large amounts of misregistration.

The results can also be interpreted further by considering the reflectance spectra of the target vehicles shown in Figure 5. It is observed that the spectra have more distinctive characteristics in the VIS (0.4 to 0.7 microns) than in the NIR (0.7 to 1.1 microns). That is, there are distinctive peaks at 0.48 microns for the blue vehicle and 0.52 microns for the green vehicle, and a unique sharp rise at 0.42 microns followed by a fairly flat region for the white vehicle. While there are differences in the overall slopes for the vehicle reflectances in NIR, there is not the same type of distinctive nature as the VIS.

In examining the detection results, we see that the VIS alone performance exceeds the NIR alone performance for vehicles of all colors when using the ASD and ACE algorithms. Note that these algorithms use background information, suggesting that the VIS spectral region has more features in the background that can be used to improve detection performance. SAM, on the other hand, looks at the spectral similarity between the pixel of interest and the true target spectrum without the use of background information. With SAM, we see the NIR region alone does slightly better than the VIS for the blue and the green vehicle, but the white vehicle results are higher for VIS than NIR, consistent with the results of the ASD and ACE algorithms. This result suggests the NIR region of the blue and green vehicles has greater contrast in spectral angle with non-target pixels than the VIS region.

While these general trends were observed in this study, it must be cautioned that the performance in given situations can vary widely depending on the particular target of interest and background characteristics and may not allows follow these same trends. Nonetheless, these observations should contribute to the overall body of understanding.

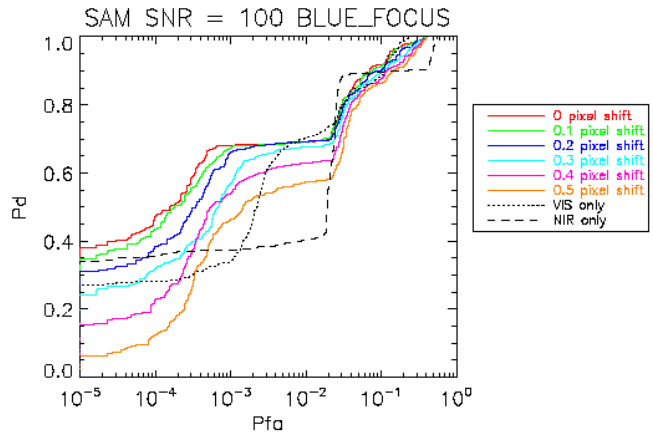

Fig. 6. ROC curves for blue vehicle using SAM algorithm. The vertical axis is the probability of detection (Pd) while the horizontal axis is the probability of a false alarm (Pfa).

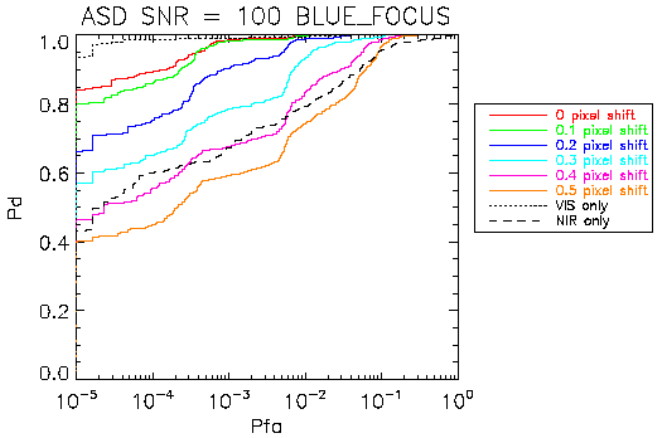

Fig. 7. ROC curves for blue vehicle using ASD algorithm. The vertical axis is the probability of detection (Pd) while the horizontal axis is the probability of a false alarm (Pfa).

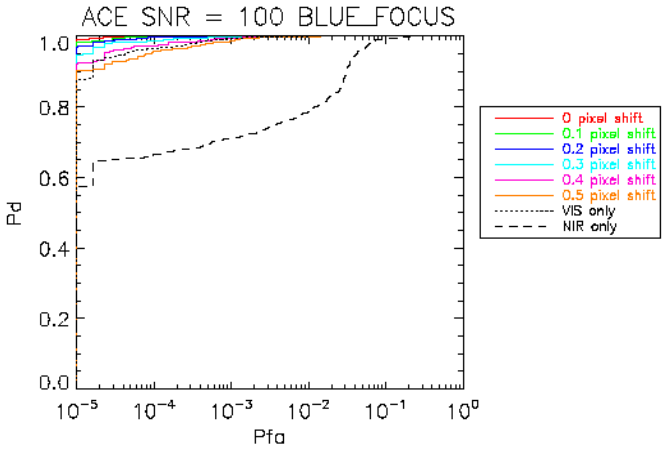

Fig. 8. ROC curves for blue vehicle using ACE algorithm. The vertical axis is the probability of detection (Pd) while the horizontal axis is the probability of a false alarm (Pfa).

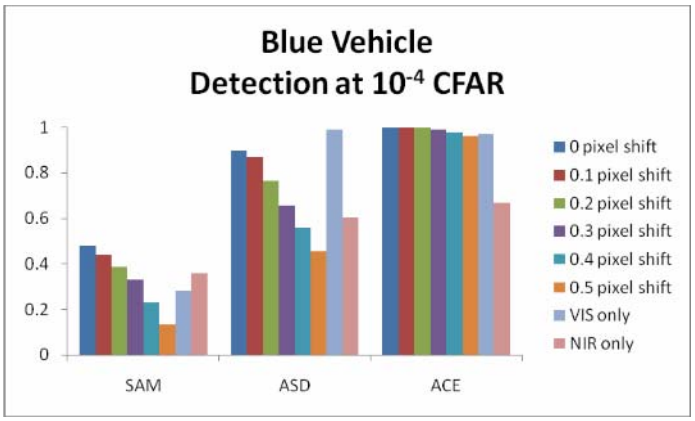

Fig. 9. Detection rates at CFAR=10^{-4} for the blue vehicle

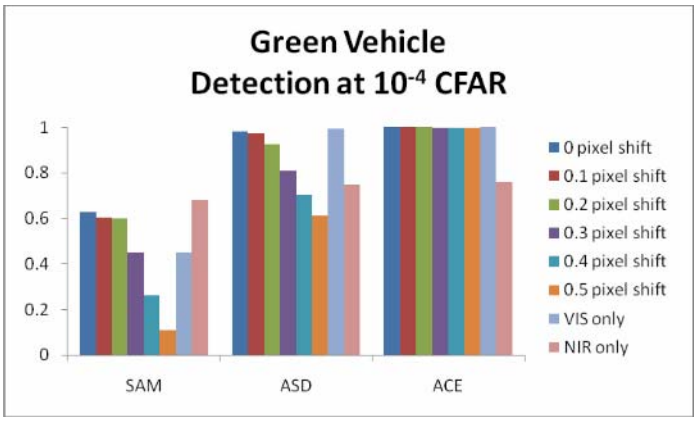

Fig. 10. Detection rates at CFAR=10^{-4} for the green vehicle

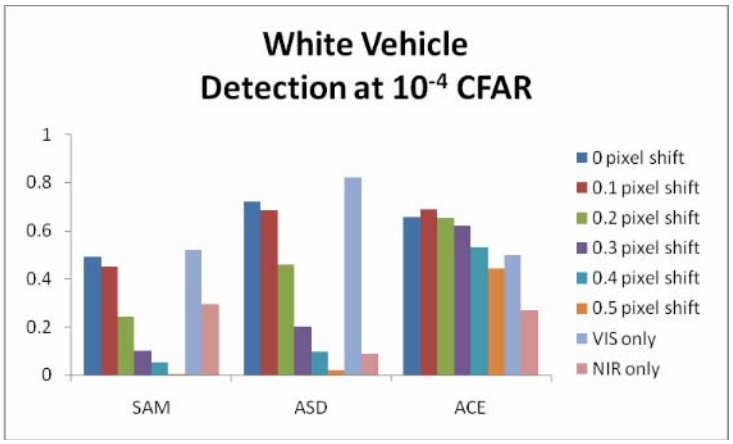

Fig. 11. Detection rates at CFAR=10^{-4} for the white vehicle

5 CONCLUSIONS

The results from this experiment show that the statistical algorithm ACE is more robust than the geometric algorithms SAM and ASD in the presence of band-to-band misregistered hyperspectral data. While the overall detection rates for ACE were not necessarily higher than those for ASD, the ACE detection rates operating on full spectrum misregistered data were often higher than detection rates using VIS or NIR bands separately. This result indicates that statistical approaches may be useful for target detection applications when using hyperspectral data with unknown amounts of misregistration between spectral bands.

Acknowledgments

We acknowledge our Air Force Research Laboratory Program Manager, Dr. Devert Wicker, for his support and guidance throughout this project. This material is based on research sponsored by AFRL/RYAT under agreement number FA8650-04-1-1717 (BAA 04- 03-SNK Amendment 3). The U.S. Government is authorized to reproduce and distribute reprints for Governmental purposes notwithstanding any copyright notation thereon. The views expressed in this article are those of the authors and do not reflect the official policy or position of the United States Air Force, the Department of Defense, or the U.S. Government.

References

[1] C. Simi, A. Hill, H. Kling, C. LaSota, J. Zadnik, J. Parish, and J. Beaver, "Night vision imaging spectrometer (NVIS) calibration and configuration: recent developments," *Proc. SPIE* **4381**, 109-117 (2001) [doi: 10.1117/12.436998].

[2] J. Schott, T. Gallagher, B. Nordgren, L. Sanders, and J. Barsi, "Radiometric calibration procedures and performance for the modular imaging spectrometer instrument (MISI)," *Proc. Earth Int. Airborne Rem. Sens. Conf.*, ERIM, Ann Arbor, MI (1999).

[3] J. Pearlman, P. Barry, C. Segal, J. Shepanski, D. Beiso, and S. Carman, "Hyperion, a space-based imaging spectrometer," *IEEE Trans. Geosci. Rem. Sens.* **41**, 1160-1173 (2003) [doi: 10.1109/TGRS.2003.815018].

[4] F. Dell'Endice, J. Nieke, D. Schläpfer, and K. Itten, "Scene-based method for spatial misregistration detection in hyperspectral imagery," *Appl. Opt.* **46** (15), 2803-2816 (2007) [doi:10.1364/AO.46.002803]

[5] H. van Trees, *Detection, Estimation and Modulation Theory, Part I*, Wiley, New York(1968).

[6] J. Casey, "A comparative analysis of hyperspectral target detection algorithms in the presence of misregistered data," M.S. Thesis, Chester F. Carlson Center for Imaging Science, *Rochester Institute of Technology* (2008).

[7] J. R. Schott, S. D. Brown, R. V. Raqueño, H. N. Gross, and G. Robinson, "An advanced synthetic image generation model and its application to multi/hyperspectral algorithm development," *Can. J. Rem. Sens.* **25** (2), 99-111 (1999).

[8] A. Berk, L.S. Bernstein, G.P. Anderson, P.K. Acharya, D.C. Robertson, J.H. Chetwynd and S.M. Adler-Golden, "MODTRAN Cloud and Multiple Scattering Upgrades with Application to AVIRIS," *Rem. Sens. Environ.* **65**, 367-375 (1998) [doi: 10.1016/S0034-4257(98)00045-5].

[9] E. Ientilucci and S. Brown, "Advances in wide area hyperspectral image simulation," *Proc. SPIE* **5075**, 110-121 (2003) [doi: 10.1117/12.488706].

[10] G. Smith and E. Milton, "The use of the empirical line method to calibrate remotely sensed data to reflectance," *Int. J. Rem. Sens.* **20**, 2653-2662 (1999) [doi:10.1080/014311699211994]

[11] F. Kruse, A. Lefkoff, J. Boardman, K. Heidebrecht, A. Shapiro, P. Barloon, and A. Goetz, "The spectral image processing system (SIPS)-interactive visualization and analysis of imaging spectrometer data," *Rem. Sens. Environ.* **44**, 145-164 (1993) [doi:10.1016/0034-4257(93)90013-N]

[12] S. Kraut, L. Scharf, and L. McWhorter, "Adaptive subspace detectors," *IEEE Trans. Signal Process.* **49**(1) 1-16 (2001)[doi:10.1109/78.890324]

[13] E. Conte, M. Lops, and G. Ricci, "Asymptotically optimum radar detection in compound-Gaussian clutter," *IEEE Trans. Aerospace Electron. Syst.* **31** (2) 617-625 (1995) [doi:10.1109/7.381910]

[14] D. Manolakis and G. Shaw, "Detection algorithms for hyperspectral imaging applications," *IEEE Signal Process. Mag.* **19** (1) 29-43 (2002) [doi: 10.1109/79.974724].

Jason T. Casey received his BS degree from the State University of New York Geneseo in 2005 and his MS in Imaging Science from the Rochester Institute of Technology in 2008. He is currently employed at Logos Technologies in Arlington, Virginia.

John P. Kerekes received his BS, MS, and PhD degrees in Electrical Engineering from Purdue University in 1983, 1986, and 1989, respectively. From 1989 to 2004 he was employed as a member of the Technical Staff at the Massachusetts Institute of Technology's Lincoln Laboratory where he performed research and development in the modeling and analysis of optical and microwave remote sensing systems. Since 2004 he has been employed as an Associate Professor in the Chester F. Carlson Center for Imaging Science at the Rochester Institute of Technology. His research interests continue to be in the development and use of spectral imaging and other remote sensing technologies for the extraction of information from remotely sensed measurements. He is a Senior Member of the IEEE, and a member of SPIE, OSA, AGU, ASPRS, and AMS.